AIAA 81-0068R

Characteristics of Mean Velocity in the Tip Region of Turbomachinery Rotor Exit

R. M. Davino* and B. Lakshminarayana†
The Pennsylvania State University, University Park, Pa.

This paper reports the experimental study of the three-dimensional characteristics of the mean velocity in the annulus-wall boundary layer and wake mixing region of a moderately loaded compressor rotor blade. The measurements reported were obtained using a three-sensor hot-wire probe at the exit of the rotor. They consisted of tangential surveys at several axial and radial locations downstream of the compressor rotor blade passage. The variation of the streamwise, normal, and radial velocity profiles and their decay characteristics are derived from this data. The measurements reveal the highly complex and three-dimensional nature of the annulus-wall flowfield and the nature of the interaction of the annulus-wall boundary layer, the blade boundary layers and wake, and the secondary flow associated with the tip region.

Nomenclature

c = blade chord length
L = semiwake width (tangential distance in the wake between points where the velocity defect is half the maximum defect)
R = radius ratio (r/r_t)
(r,θ,z) = radial, tangential, and axial coordinates, Fig. 1
S = blade spacing
(s,n,r) = streamwise, normal, and radial coordinate directions, Fig. 1
U_t = peripheral speed of the rotor blade
W = relative flow velocity, Fig. 1
w = defect in relative mean velocity
Y = tangential distance behind the rotor
Z = axial distance from the rotor blade trailing edge normalized by the local rotor blade chord, Fig. 1
α = flow angle measured from the axial direction, Fig. 1
β = meriodonal (radial) flow angle measured from the reference streamline at the midpassage, Fig. 1
θ^* = momentum thickness of the boundary layer, Eqs. (1) and (2)
ρ = fluid density
Ω = rotational speed of the rotor blade

Subscripts

c = center of blade wake
0 = freestream value
ps,ss = pressure and suction side of the rotor blade wake, respectively
(s,n,r) = values in the streamwise, normal, and radial directions, respectively
t = blade tip location
(z,θ,r) = values in the axial, tangential, and radial directions, respectively

Superscript

$(\bar{\ })$ = passage-averaged value

Introduction

THE flow near the tip region of a compressor rotor is extremely complicated due to the interaction of the secondary flow, annulus wall boundary layer, blade boundary layer (or wake), tip leakage flow, and scraping vortex flow. These flows are illustrated schematically in Fig. 1. All the investigations carried out hitherto[1,2] are confined to a study of one of these phenomena in the absence of the other effects. A systematic program is underway at The Pennsylvania State University to study the tip end wall flows in a rotor where all these flows interact to produce a complex flowfield. The measurements taken at the exit of the rotor near the tip end wall region is reported in this paper. The rotor wake is found to dominate the flowfield in this region.

The study of rotor wakes and the endwall flow in the annulus wall region is important for establishing improved aerodynamic design criteria and efficiency, for predicting noise levels, and for determining the stall, surge, vibration, and flutter characteristics of turbomachinery. Mixing of the end wall flow (annulus wall boundary layer, rotor wake, secondary flow, blade boundary layer, etc.) with the freestream and the annulus wall represents a dissipation of energy and, therefore, a source of loss in efficiency. In view of the three dimensionality of the rotor wake and its dependency on a large number of parameters, both an analytical and an experimental investigation of the rotor wake in the end wall flow region are extremely difficult. Earlier data on the rotor wake[3,4] were taken from a lightly and a moderately loaded rotor near the midspan regions, where the annulus wall boundary-layer effects are negligible. The objective of the

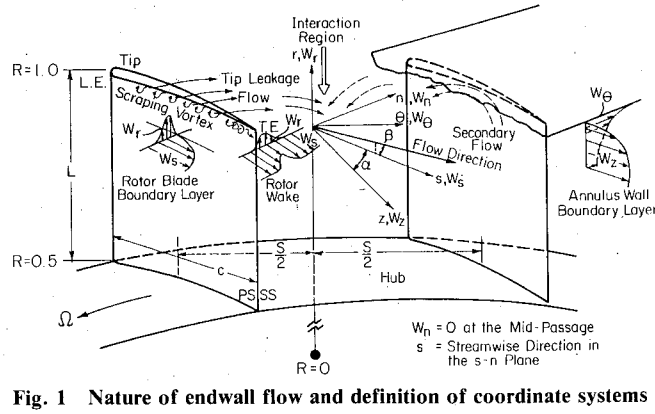

Fig. 1 Nature of endwall flow and definition of coordinate systems used.

Presented as Paper 81-0068 at the AIAA 19th Aerospace Sciences Meeting, St. Louis, Mo., Jan. 12-15, 1981; submitted March 10, 1981; revision received Aug. 26, 1981.

*Department of Aerospace Engineering; presently, Aeroacoustics Engineer, General Electric Company, Evendale, Ohio. Member AIAA.

†Director of Computational Fluid Dynamics Studies and Professor of Aerospace Engineering. Associate Fellow AIAA.

present paper is to study the flow only in the annulus wall region.

This paper reports some results of a comprehensive investigation of the rotor wake and the end wall region flow near the annulus wall of a moderately loaded compressor rotor. One aspect of this investigation will be discussed; a detailed study of the structure and decay characteristics of the mean velocity profiles of the rotor wake in the annulus-wall boundary layer and the wake mixing region of the rotor exit. The data presented in this paper represent the first set of comprehensive measurements obtained near the end wall region at the exit of a compressor rotor blade passage. This is a companion paper of Ref. 5 where the turbulence properties of the wake and its decay characteristics are discussed.

Test Facility, Data Acquisition, and Procedures

The measurements reported in this paper were performed using the axial flow compressor facility located in the Turbomachinery Laboratory of The Pennsylvania State University. The measurements were acquired employing a three-sensor hot-wire probe placed behind the rotor blade row using a probe traverse mechanism mounted on the annulus wall. From these measurements, information on the mean velocity, turbulence intensity, Reynolds stress, and various other characteristics of the flow in the rotor exit annulus wall region were determined.

Axial Flow Compressor Facility

A general description of the compressor stage is given by Smith,[6] and a detailed discussion of the facility is given by Lakshminarayana.[7] Good peak efficiencies are exhibited by the rotor. The hub/annulus wall diameter ratio of the facility is 0.5, with the diameter of the annulus wall equal to 0.932 m. The inlet guide vane row, which consists of 43 blades, is followed by the 21-bladed rotor. The rotor is driven by a 37.29-kW variable speed motor through a belt and pulley system. The rotor is followed by a stator vane row of 25 blades. The axial spacing between the rotor and stator blade rows is approximately four rotor chord lengths at the blade tip. Downstream of the stator is located a Joy axial flow fan with variable blade setting for the variation of pressure rise and mass flow. The facility is terminated downstream by an aerodynamically designed throttle which provides additional control of the stage operating characteristics. Some of the other operating conditions and rotor specifications are as follows: inlet velocity, 29.04 m/s; flow coefficient based on tip speed, 0.56; stage loading coefficient based on tip speed, 0.4864; speed of rotor, 1066 rpm; and tip clearance, 0.25-0.3 cm. Blade element data at the tip are: NASA 65 series blade section, chord 15.41 cm, spacing 13.94 cm, maximum thickness 5.10% of chord, stagger angle 45.0 deg, and camber 8% of chord. The blade profile near the tip section is given in Refs. 6 and 7.

Probe Instrumentation and Data Transmission System

A triaxial hot-wire probe, similar to that used in Refs. 3 and 4, was employed for all measurements reported in this paper. The probe sensors were built out of tungsten wire and had a length-to-diameter ratio of 300. The probe calibration, performed employing a low-turbulence facility, was corrected for yaw and pitch angle sensitivity, temperature variation, and aging of the sensor.

The stationary probe measurement technique employed was developed by Poncet and Lakshminarayana[8] and the improved version is described in Ref. 9. The sensors were connected to three DISA 55M10 constant-temperature anemometer units. The fluctuating ac signals were amplified and recorded with a SAVRE IV fm signal recorder/reproducer at a tape speed of 38.1 cm/s. The center frequency of recording was 43 kHz, and the frequency of the signals could vary from 0 to 10 kHz. A specific circumferential position behind the rotor was identified by referring to a pulse generator that was installed on the compressor axis. This pulse generator provided one sharp pulse for each revolution of the rotor row. Each of the rotor passages could be identified with the pulse signal. An ensemble average was obtained for the specific passage flow of interest. Due to the high-rotational speed of the rotor (1066 rpm) and number of rotor blades (21), one survey of a blade passage requires very little time (0.0027 s). This gives an impractically high sampling speed; therefore, the analog signal was digitized at 1/16 real time. The H.P. 7900 A.D.C. unit was used for this analog-to-digital conversion. The digitizing was performed at a tape reproduction speed of 2.38 cm/s. The instantaneous flow velocity was obtained from the cooling velocities of the three sensors using hot-wire equations. The various mean and turbulent flow characteristics in the rotor frame of reference were obtained statistically with these instantaneous velocities. A detailed discussion of the data processing procedure is given by Reynolds and Lakshminarayana.[3]

Experimental Results and Interpretation

The data processing procedure just described provided sufficient information to derive the three components of mean velocity and the six components of turbulence stress (including normal stress) in the relative frame of reference. These quantities were derived in the (s,n,r) coordinate system shown in Fig. 1. The orientation of this coordinate system, as well as the flow angle α, with respect to the compressor coordinate system (z,θ,r), is indicated. The (s,n,r) coordinate system follows the projection of the flow at the midpassage in the radial plane for the various axial measurement locations. The reported measurements consist of tangential surveys behind the rotor blade passage at various axial and radial locations. The probe was positioned at a circumferential position between IGV wakes. These locations are listed in Table 1. The axial distance behind the blade trailing edge is normalized by the rotor blade chord length at the specified radius. The radial distance from the compressor axis is normalized by the radial distance to the blade tip.

Mean Velocity Profiles

Tangential surveys of the three components of mean velocity at various radial and axial locations are presented in the following sections. These profiles present a radial and circumferential variation of the flowfield at each axial location. These measurements are presented as a continuous profile (300 points across the passage) due to the data acquisition and reduction technique. The three components of relative mean velocity are normalized with respect to the corresponding maximum streamwise velocity in the freestream. Table 1 provides values of this streamwise velocity in the freestream at the measurement locations. The tangential distance behind the rotor passage is normalized by the local blade spacing. The pressure and suction sides of the wake (as referenced to the rotor blade) are indicated with a tangential distance of $Y=0$ specifying the wake center. A tangential distance of $Y=0.5$ indicates midpassage.

Table 1 Maximum streamwise velocity for the reported measurement stations [values of (W_{s0}/U_t)]

Z / R	Exit flow 0.021	0.042	0.125	0.458	% span from tip
0.986	0.514	0.527	0.429	0.318	2.8
0.980	0.554	0.559	0.490	0.373	4.0
0.973	0.573	0.580	0.531	0.425	5.4
0.959	0.548	0.573	0.547	0.479	8.0
0.945	0.563	0.531	0.547	0.531	11.0
0.918	0.591	0.542	0.547	0.528	16.0
0.891	0.588	0.558	0.527	0.518	22.0

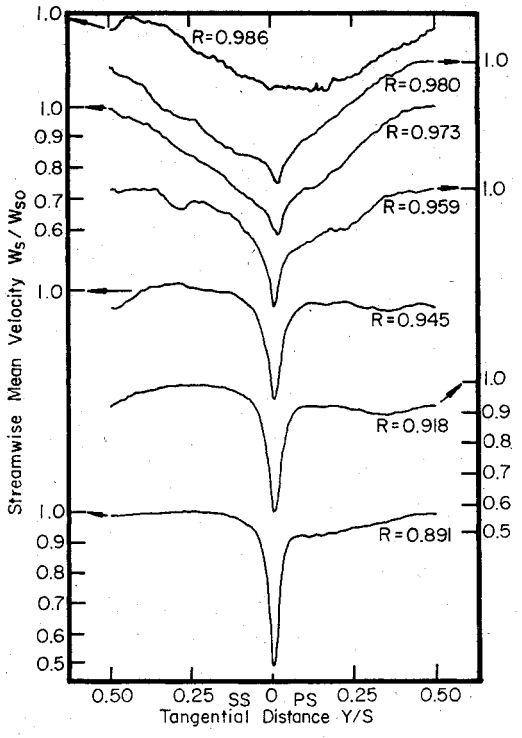

Fig. 2 Streamwise mean velocity profiles at various radial locations, $Z = 0.021$.

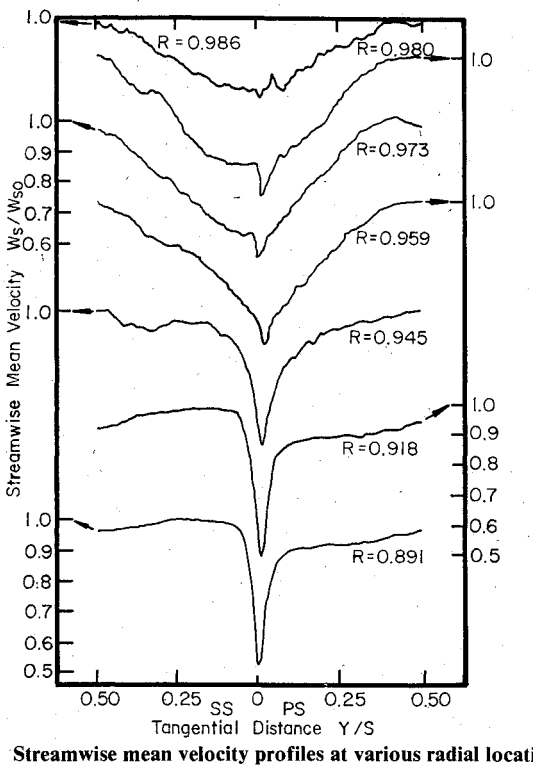

Fig. 4 Streamwise mean velocity profiles at various radial locations, $Z = 0.125$.

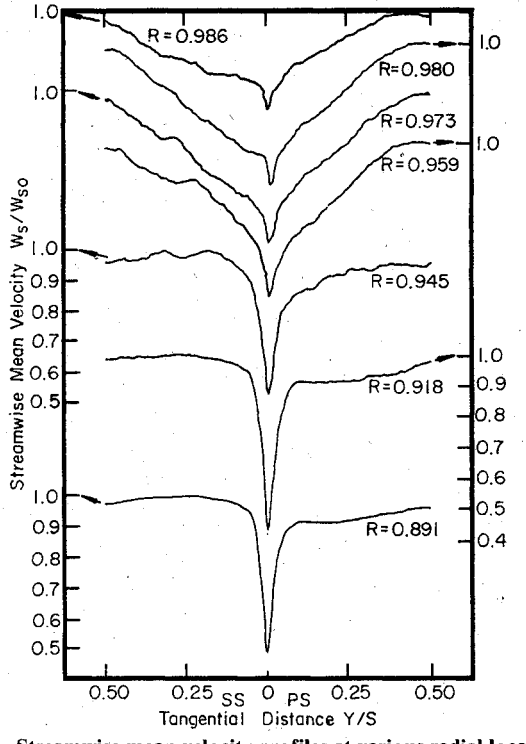

Fig. 3 Streamwise mean velocity profiles at various radial locations, $Z = 0.042$.

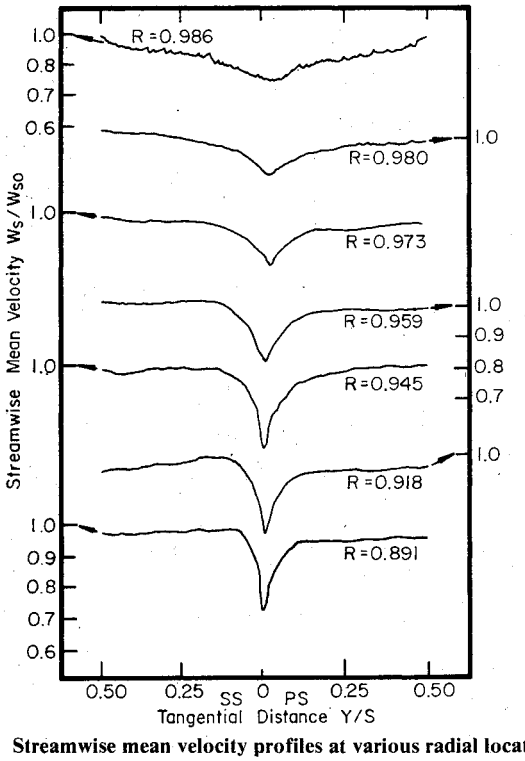

Fig. 5 Streamwise mean velocity profiles at various radial locations, $Z = 0.458$.

Streamwise Mean Velocity

The circumferential variation of the streamwise velocity at the various axial and radial locations behind the blade row is presented in Figs. 2-5. The dominant feature of these profiles is the character of the rotor blade wake and its interaction with the annulus wall flowfield. At radial locations below $R = 0.945$, there is little flow interaction and the wake profiles are defined clearly. These wake profiles are asymmetrical about the wake center, indicating the differential growth of the boundary layers on the two surfaces of the rotor blade. This is to be thicker than the pressure-surface boundary layer. The asymmetry is maintained even at the last axial location, which is approximately one-half chord downstream of the rotor blade trailing edge and is observed even in the normal and radial velocity profiles. The pressure gradient across the blade passage is also shown to exist immediately downstream of the blade trailing edge. This is reflected in the freestream velocity distributions of Figs. 2-5. The streamwise velocity is

greater on the suction side of the wake than on the pressure side of the wake. This effect persists to approximately one-half chord downstream of the blade row.

For the radial locations at $R=0.945$ and above, the rotor blade exit flow interacts strongly with the annulus wall boundary layer. This is a region of predominantly viscous flow. The blade passage flow with a region of velocity deficit combines with the blade boundary layers and the annulus wall boundary layer. This flow interaction results in a marked decrease in velocity across the entire passage behind the rotor blade, which encompasses more tangential distance with increasing radial location. The merger of the blade boundary layer with the annulus wall boundary layer results in a large increase in the wake width as the annulus wall is approached. This trend is observed at all axial locations behind the rotor. The passage is covered entirely by the boundary layer and wake beyond $R=0.945$. This tendency is due to the radially outward transport of mass, momentum, and energy in the blade boundary layer and is also observed in the normal and radial component of wake profiles. This radially outward flow interacts with the annulus wall boundary layer to create a region of considerable flow mixing in the blade wake.

The effect of radial location upon the wake defect (w_s/W_{s0}) is seen from Figs. 2-5. At the axial location $Z=0.021$, the wake defect is 0.51 at $R=0.891$, which reduces to 0.25 at $R=0.986$. This trend is similar for all the axial locations.

The development of the blade wake near the annulus wall in the axial direction can be seen in Figs. 2-5. For the wake near the trailing edge, the velocity gradients in the tangential direction are very large. The steep gradient at the lower radial locations represents highly unstable and developing flow conditions. The gradient becomes smaller as the flow moves downstream, because of the wake spreading and mixing with the freestream. At radial locations above $R=0.945$, the wake covers the entire blade passage and, hence, reflects the effect of the complex flow interactions. In this region, the wake also decays with axial distance. A wake defect of $w_s/W_{s0}=0.25$ at $R=0.986$ and $Z=0.021$ decays to 0.15 at $Z=0.458$. This decay is due to the wake mixing with the freestream and the annulus wall boundary layer.

The maximum defect in streamwise velocity is greater at the lower radial location of $R=0.945$ than at the tip. This indicates the faster decay rate of the wake near the blade tip and presumably is caused by the flow mixing described earlier. A comparison of Figs. 2 and 5 shows that the wake near the tip decays faster than the wake at lower radii.

Normal Mean Velocity and Exit Flow Angle α

The circumferential variation of the normal velocity at various radial locations downstream of the rotor passage at $Z=0.021$ is given by Fig. 6. The profiles at other axial locations can be found in Ref. 10. The exit flow exhibits inviscid trends below the radial location of $R=0.945$. The magnitude of normal velocity increases sharply at the tangential location of the wake and then gradually decays with axial distance.[10] A normal velocity (W_n/W_{s0}) of 0.17 at $R=0.891$ and $Z=0.021$ decreases to 0.07 at $Z=0.458$. The diffusion and dissipation of the flow is due to the wake mixing with the freestream flow. The normal velocity in the wake increases with radial location. This increase is due to the increase of the boundary layers on the blade surface. Possible additional effects are due to the annulus wall boundary layer and the tip leakage flow.

Figure 6 reveals a very interesting fact. As with the streamwise and radial mean velocity profiles of the exit flow, the normal velocity profiles do not indicate the presence of the tip leakage vortex. An unsteady flow phenomena at frequencies other than the blade passing frequency could not be determined through an ensemble-average technique of data reduction. This technique was employed for the stationary probe data obtained in the rotor exit-flow region. Thus, the tip leakage vortex would not be discerned from the data, if it

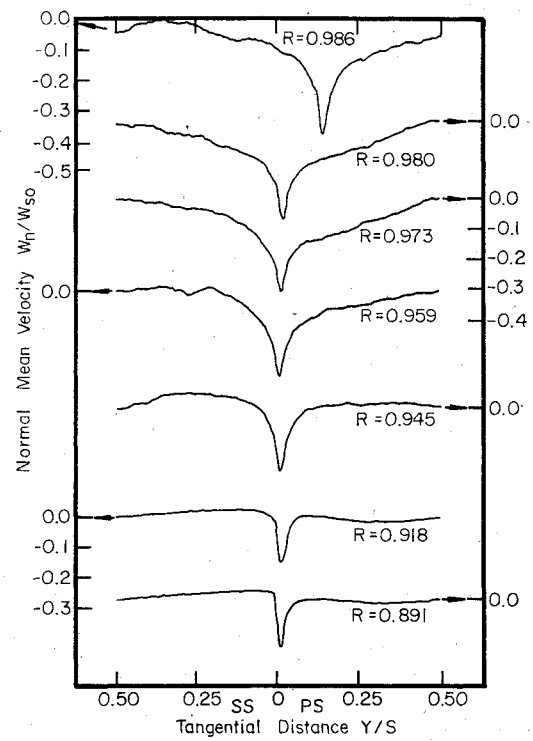

Fig. 6 Normal mean velocity profiles at various radial locations, $Z=0.021$.

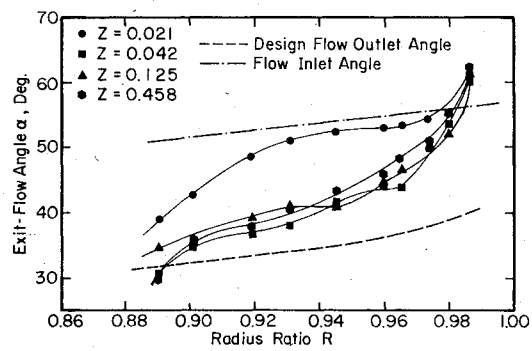

Fig. 7 Radial variation of the exit flow angle at the midpassage.

was unsteady in nature. The formation and roll up of the tip leakage flow could be unsteady in nature due to nonuniform rotor tip clearance and nonidentical blade spacing. If this condition existed, it would be difficult to discern the tip leakage vortex in the exit data.

Figure 7 shows the variation of the exit-flow angle at a circumferential location midway between blades for various radial and axial locations. The effect of the annulus wall boundary layer is seen at the blade tip, where the flow angle of the relative flow remains about the same with axial distance. The design outlet flow angle as well as the inlet flow angle are shown compared with the measured values in Fig. 7. It is evident that the flow is underturned significantly at all locations, with the maximum value occurring near the tip. The angle α varies considerably between trailing edge and far downstream. The relative flow turning is almost zero for $R>0.98$, about 2% of the span near the tip.

Radial Mean Velocity

Radial velocities in a blade row are caused by an imbalance in the radial pressure gradient and the centrifugal forces. Physically, at either surface of the rotor blade the radial velocities must be zero. The maximum radial velocities occur slightly away from the blade surface in the blade boundary

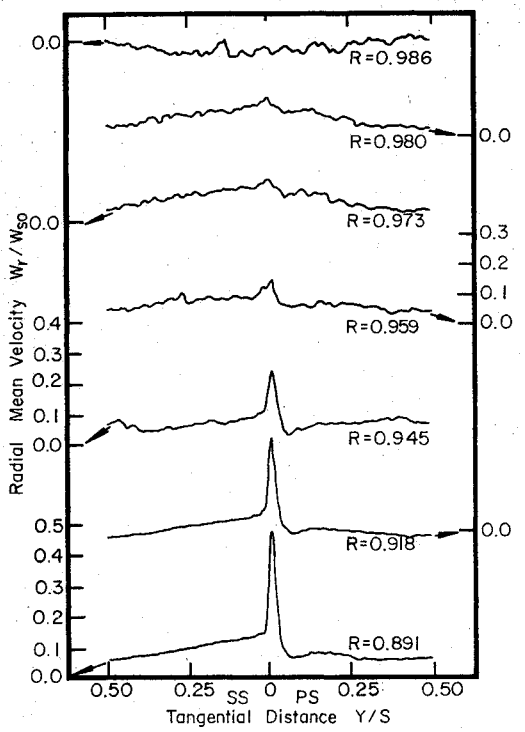

Fig. 8 Radial mean velocity profiles at various radial locations, $Z=0.021$.

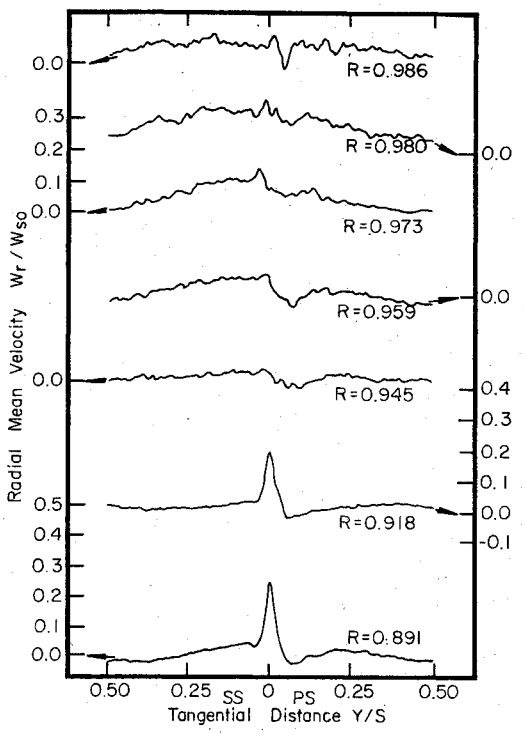

Fig. 10 Radial mean velocity profiles at various radial locations, $Z=0.125$.

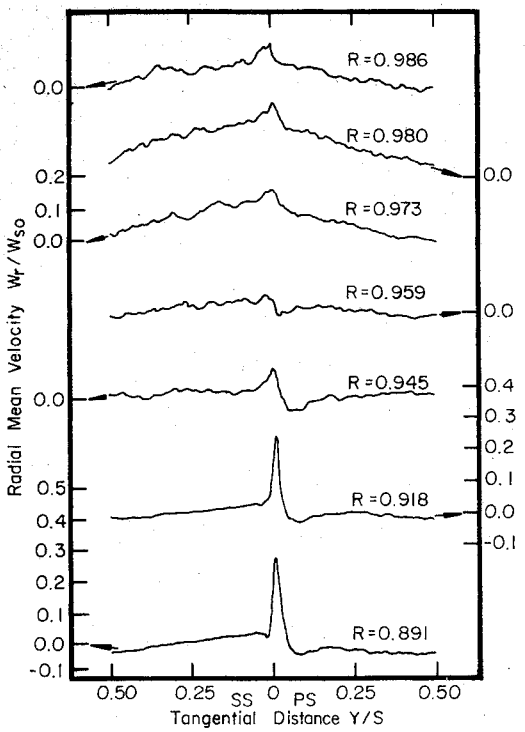

Fig. 9 Radial mean velocity profiles at various radial locations, $Z=0.042$.

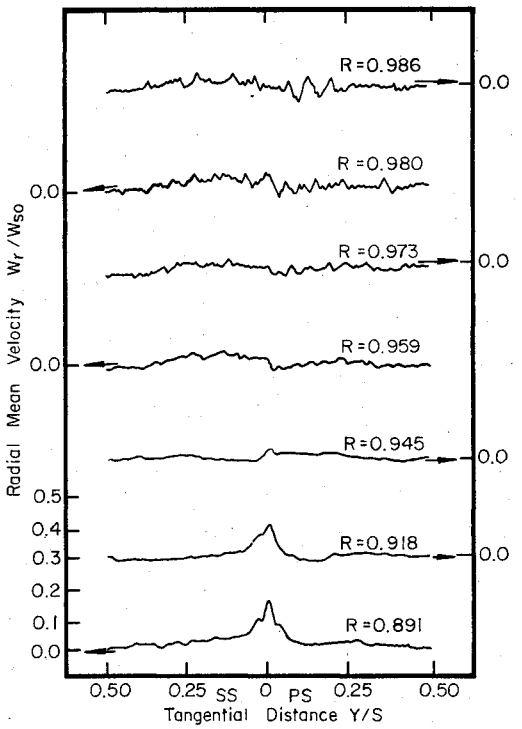

Fig. 11 Radial mean velocity profiles at various radial locations, $Z=0.458$.

layer or the wake. The radial velocity in a compressor rotor is outward due to the centrifugal force.

The radial velocity profiles given in Figs. 8-11 show the radial outward flow in the blade wake which results from the shedding of the blade boundary layers. The radially outward flow in the wake decreases rapidly in the radial direction as the annulus wall is approached. At the axial location of $Z=0.021$, the maximum radial velocity (W_r/W_{so}) of 0.40 in the wake center reduces to nearly zero values at $R=0.973$. This rapid decrease of the radial velocity is also present at the other axial locations downstream of the rotor. The interaction and subsequent mixing of the radial velocity in the wake with the annulus wall boundary layer is the cause of this rapid decrease. The radial velocity profile in the wake is seen to decay rapidly with axial distance. At $R=0.891$ and $Z=0.021$, a radial velocity (W_r/W_{so}) of 0.40 decays to 0.12 at $Z=0.458$. This decay rate is more rapid at higher radial locations where it is accelerated by the mixing of the blade wake and the

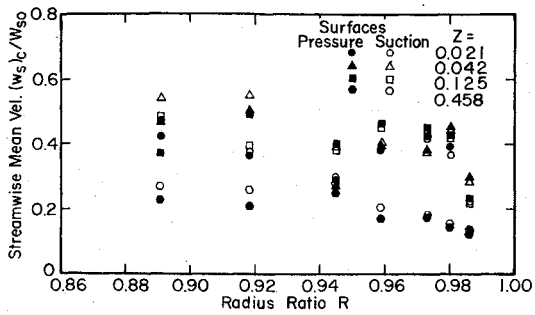

Fig. 12 Radial and axial variation of the streamwise mean velocity defect.

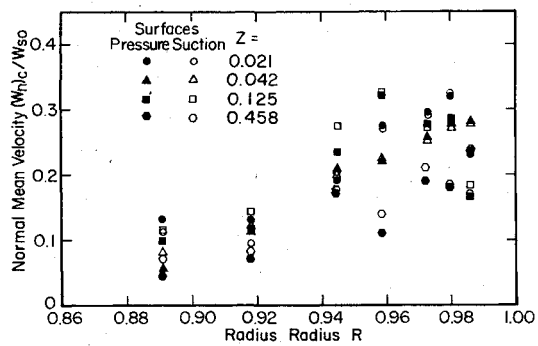

Fig. 13 Radial and axial variation of the normal mean velocity at the wake center.

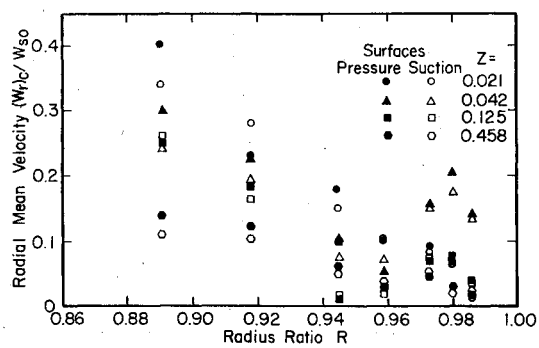

Fig. 14 Radial and axial variation of the radial mean velocity at the wake center.

annulus wall boundary layer. The radial velocity in the freestream behind the blade is zero.

It is evident that the wake type of profile dominates until $R=0.945$, beyond which the annulus wall boundary layer has a significant effect. Rapid decrease in radial velocity toward the tip brings about a rapid increase in the wake width or the blade boundary layer thickness as evidenced by Figs. 2-5.

Maximum Value or Defect in Mean Velocities at Wake Centerline

The variation of the velocity at the wake centerline reflects the decay rate or modification of the rotor wake. The decay of the mean velocity defect is influenced greatly by the pressure gradients and turbulence fluctuations downstream of the blade passage. The annulus wall boundary layer, secondary flow, and tip leakage flow in the annulus wall region also contribute to the variation of the wake profile.

The variation of the velocity at the wake centerline for the three mean velocity components is shown plotted in Figs. 12-14. Due to the asymmetric nature of the wake profiles, the velocity defect with respect to both the pressure and suction sides of the wake is plotted. The variation of the wake velocity defect in the radial and axial directions is evident. Figure 12

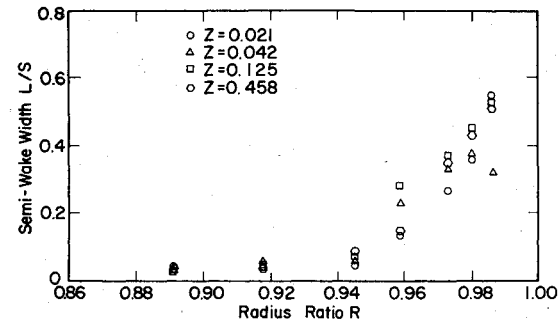

Fig. 15 Variation of the semiwake width with axial distance.

shows this variation for the maximum streamwise mean velocity defect $(w_s)_c/W_{s0}$. The wake decay is maximum near the blade tip. This is brought about by the tip clearance flow, annulus wall boundary layer, and secondary flow that are prevalent in this region. The general trend observed is that the velocity defect decays rapidly in the axial direction. This trend is most pronounced at the lower radial locations ($R=0.89$, 0.92), where a velocity defect of $(w_s)_c/W_{s0}=0.55$ decays to 0.25 over an axial distance of half a blade chord. This rapid decay is attributed to large turbulence intensities, pressure gradients, and three-dimensional effects. The velocity defect increases slightly from $Z=0.02$ to $Z=0.04$ near $R=0.9$, beyond which there is a monotonic decrease. The exact reason for this is not known. At higher radial locations the streamwise velocity defect of $(w_s)_c/W_{s0}=0.25$ near the blade trailing edge decays to 0.12 at $Z=0.458$. The shape of the profiles and the velocity defect at the radial locations above $R=0.945$ are due to the highly three-dimensional, viscous nature of the flow. The interaction of the annulus wall boundary layer with the exit flow induces a broader wake profile which extends over the entire blade spacing. This flow interaction dissipates the strong velocity gradients present in the wake trailing-edge region. The dissipation of the wake produces lower values of the streamwise velocity defect.

The variation of the maximum normal mean velocity $(W_n)_c/W_{s0}$ in the radial and axial directions is presented in Fig. 13. A substantial decay of the velocity is observed from the blade trailing edge to the downstream locations. This decay is due to flow mixing and wake spreading as the wake travels downstream. With increasing radius, the normal velocity increases due to the viscous nature of the annulus wall boundary layer and the presence of the tip leakage flow in the normal direction. This increases the normal velocity of the wake in this region. It is also evident from Fig. 7.

Figure 14 shows the variation of the maximum radial mean velocity $(W_r)_c/W_{s0}$ in the radial direction and as the flow propagates downstream. The velocity is seen to decrease very rapidly with axial distance. At $R=0.891$, a radial velocity of $(W_r)_c/W_{s0}=0.40$ at $Z=0.21$ decays to 0.14 at $Z=0.458$. This rapid decay rate is also observed at higher radial locations, with a decrease in the decay rate as the blade tip is approached. The high levels of turbulence and viscous effects in this region promote a rapid decay rate. The radial velocity is also seen to decrease rapidly in the radial direction. This is due to the presence of the annulus wall boundary layer and its viscous nature, which induces rapid flow mixing in the radial direction.

Semiwake Width (L)

The variation of the semiwake width L ($L_{ss}+L_{pp}$) with radial and axial location is shown in Fig. 15. The distance from the wake centerline to the location where the velocity defect is one-half was used as the characteristic length scales L_{ss} and L_{pp}. The semiwake width is controlled by many parameters, including the section drag coefficient, the blade spacing, and the rate of decay of the wake. In the case of a single airfoil, the wake can expand in an infinite medium. In

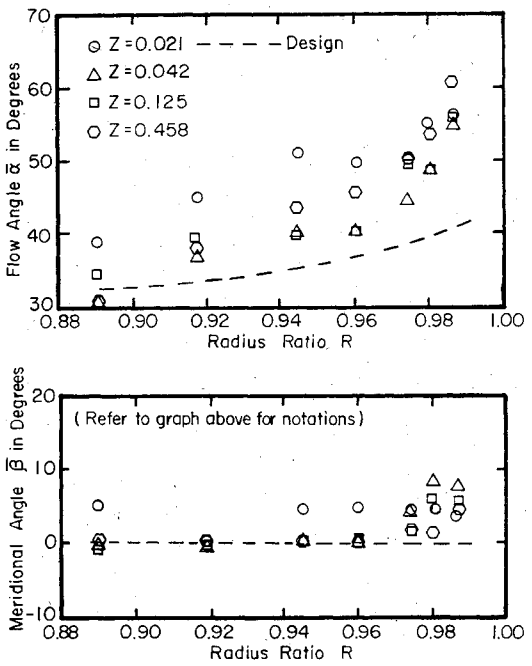

Fig. 16 Radial variation of the passage-average flow angles ($\bar{\alpha}$) and ($\bar{\beta}$) at various axial locations.

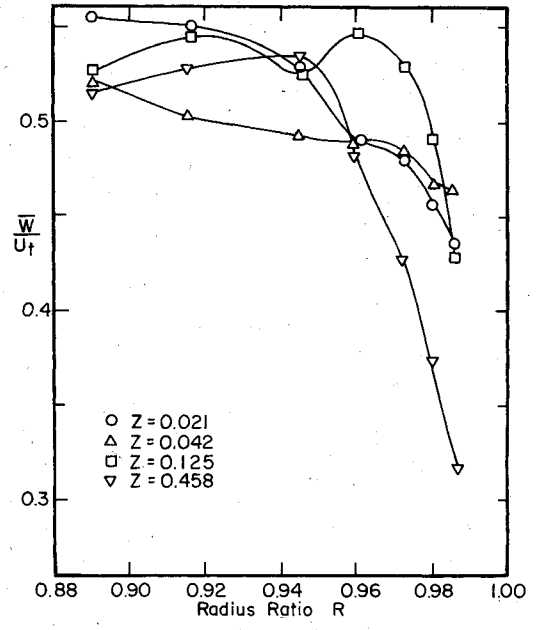

Fig. 17 Radial and axial variation of passage-averaged total relative velocity ($|\overline{W}|$) at the exit of the rotor.

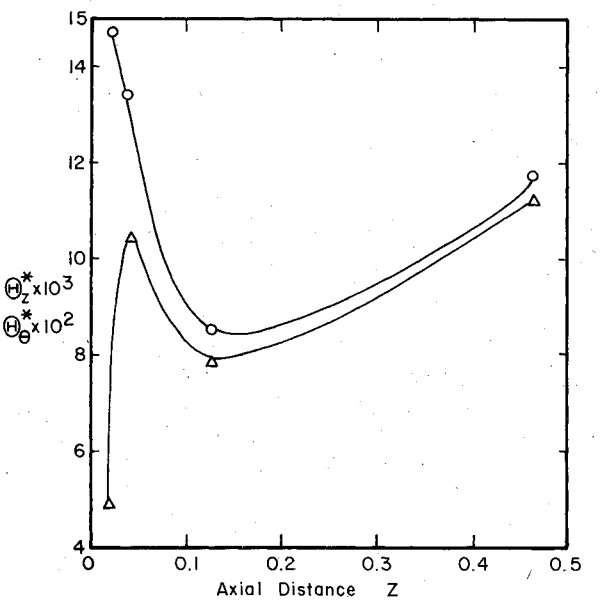

Fig. 18 Momentum thickness (Δ, Θ^*_θ; 0, Θ^*_z) variation with axial distance in the annulus wall boundary layer.

the case of a rotor, however, the wake growth is limited by the adjacent blade wakes. At radial locations below $R=0.946$, the semiwake width is seen to be only 4-5% of the blade spacing. A gradual increase in the semiwake width is also seen with axial distance.

The semiwake width is seen to increase very rapidly toward the annulus wall. This is due partially to the radial transport of mass, momentum, and energy in the rotor wake by the radial velocity. Also, the interaction of the annulus wall boundary layer with the blade wake in the interference region causes a rapid increase in the semiwake width. At radial locations near the tip, the semiwake width expands to 50% of the blade spacing. This indicates that the edge of one wake is adjacent to another. With this flow situation, it is possible that the two wakes might merge together.

Passage-Averaged Flow-Angle Variation ($\bar{\alpha}$,$\bar{\beta}$)

The radial variation of the passage-averaged flow angle $\bar{\alpha}$ and the meriodonal flow angle $\bar{\beta}$ (measured from the reference streamline at midpassage) at various axial locations is plotted in Fig. 16. The meriodonal flow angle is indicative of the magnitude of the radial velocities. The nature of these angles with respect to the streamwise coordinate system is shown in Fig. 1. Figure 16 shows that the flow angle $\bar{\alpha}$ deviates from the design value (dashed lines) considerably at radial locations near the blade tip. This trend is evident for both the blade passage flow and the blade exit flow.[10] At the lower radial locations, the flow angle deviates only slightly from the design value. However, as the radial location is increased, up to the blade tip, $\bar{\alpha}$ increasingly deviates from the design condition. At $R=0.986$, the flow is underturned by approximately 20 deg. This flow underturning is induced by the effect of the annulus wall. The absolute flow velocity decreases in the annulus wall boundary layer, resulting in the underturning of the relative flow. This effect may also be due to the leakage flow, which underturns the relative flow.

Figure 16 also shows a comparison of the meriodonal flow angle $\bar{\beta}$, which is averaged over the blade passage for the exit flow, with the design value. At the exit of the blade passage near the tip, the flow angle $\bar{\beta}$ deviates appreciably from its value near the midpassage ($\beta=0$). This seems to indicate substantial spanwise flows in this region, caused by either the leakage flow or the secondary flow or the rotor wake.

Characteristics of the Annulus Wall Boundary Layer

The radial variation of the passage total relative velocity ($\overline{W}$) at various axial locations is shown in Fig. 17. These are obtained by passage averaging the total relative velocity. The growth of the boundary layer from $Z=0.021$ to $Z=0.458$ is evident. The annulus wall boundary-layer thickness nearly doubles from $Z=0.021$ to $Z=0.458$. The boundary-layer profile is almost identical near the tip ($R>0.94$) at $Z=0.021$ and 0.042. Substantial change occurs beyond this station. This indicates that the mixing of the endwall flow is much more intense beyond the trailing edge.

The momentum thickness implies the loss of momentum in the boundary layer, as compared with the potential flow. In the case of the annulus wall region, this loss of momentum is associated with the annulus wall boundary layer and the flow interactions between the blade boundary layers, the tip leakage flow, and the secondary flow. The integration of the

momentum thickness Θ^* was performed along the radial direction and is given by

$$\Theta_z^* = \int_{R=0.891}^{R=1.0} \frac{\overline{W}_z}{\overline{W}_{z_0}} \left(1 - \frac{\overline{W}_z}{\overline{W}_{z_0}}\right) dR \quad (1)$$

$$\Theta_\theta^* = \int_{R=0.891}^{1.0} \frac{\overline{W}_\theta}{\overline{W}_{\theta_0}} \left(\frac{\overline{W}_\theta}{\overline{W}_{\theta_0}} - 1\right) dR \quad (2)$$

where $\overline{W}_z$, $\overline{W}_\theta$, are the passage-averaged axial and tangential relative velocity, respectively. $\overline{W}_{z_0}$, $\overline{W}_{\theta_0}$ are the passage-averaged axial and tangential relative velocity, respectively, at $R=0.891$, Θ^* is normalized by the tip radius. The data were extrapolated from $R=0.986$ to the annulus wall, where $\overline{W}_{\theta_0} = U_t$ and $\overline{W}_{z_0} = 0$. The variation of the annulus wall boundary-layer momentum thickness with downstream distance is shown plotted in Fig. 18. Downstream of the blade passage, the axial momentum thickness decreases and then increases with axial distance. The increase is due to the development of the annulus wall boundary layer as the flow progresses downstream. The decrease in momentum thickness (Θ_z^*) near the trailing edge is caused by complex interaction of secondary flow, leakage flow, wake, and annulus wall boundary layer in this region. The tangential momentum thickness distribution shows an irregular trend.

Conclusions

1) The exit flow from the blade passage is dominated by the development of the rotor wake at locations below 5% of the span from the tip. The region outside the wake in this region is primarily inviscid in nature. As the blade tip is approached, the streamwise velocity defect and the radial velocity in the wake decreases and the normal velocity increases. This is due to the wake mixing with the freestream and the influence of the annulus wall boundary layer. The exit flow is substantially underturned in this region.

2) Strong radial outward flows are measured within the rotor wake. These radial velocities are very high at about 10% of the span from the tip and decrease rapidly to zero near the tip. This causes rapid increase in the wake width toward the tip and encompasses the entire blade passage at the tip. The wake width increases with axial distance.

3) The decay of the blade wake is maximum near the blade tip which is due to mixing of mass, momentum, and energy with the annulus wall boundary layer. The high levels of turbulence and viscous effects in this region promote a rapid decay rate in the axial direction.

4) The momentum thicknesses of the annulus wall boundary layer increase with axial distance beyond $Z=0.125$ due to the development of the annulus wall boundary layer. A decrease in axial momentum thickness is observed in the trailing-edge region and this may have been caused by an energizing of the flow by the tip leakage flow.

Acknowledgments

This work was supported by NASA through Grant NSG 3212, with P. M. Sockol as the project monitor. The authors wish to thank G. Kane and J. Fetterolf for their aid in experimental setup and instrumentation.

References

[1] Lakshminarayana, B. and Horlock, J. H., "Secondary Flows and Losses in Cascades and Axial Flow Turbomachines," *International Journal of Mechanical Sciences,* Vol. 5, 1963, p. 287.

[2] Horlock, J. H., *Axial Flow Compressors,* R. E. Kreiger Publishing Co., New York, 1973.

[3] Reynolds, B. and Lakshminarayana, B., "Characteristics of Lightly Loaded Fan Rotor Blade Wakes," NASA CR-3188, Oct. 1979.

[4] Ravindranath, A., "Mean Velocity and Decay Characteristics of the Near and Far Wake of a Compressor Rotor," *Journal of Engineering for Power,* Vol. 102, July 1980, pp. 535-548.

[5] Davino, R. and Lakshminarayana, B., "Turbulence Characteristics in the Annulus-Wall Boundary Layer and Wake Mixing Region of a Compressor Rotor Exit," ASME Paper 81-GT-148, 1981 (to be published in *Journal of Engineering for Power,* 1982).

[6] Smith, L. H., "Three-Dimensional Flow in an Axial Flow Turbomachinery," WADC Tech. Rept. 55-348, Vol. 2, John Hopkins University, 1956.

[7] Lakshminarayana, B., "An Axial Flow Research Compressor Facility Designed for Flow Measurement in Rotor Passages," *Journal of Fluids Engineering,* Vol. 102, Dec. 1980, pp. 402-411.

[8] Poncet, A. and Lakshminarayana, B., "Three-Dimensional Analysis and Measurement of the Flow in a Three Bladed Rocket Pump Inducer," NASA CR-2290, 1973, pp. 1-126.

[9] Lakshminarayana, B., "Techniques for Aerodynamic and Turbulence Measurements in Turbomachinery Rotors," *Journal of Engineering for Power,* Vol. 103, April 1981, pp. 374-392.

[10] Davino, R., "Three-Dimensional Mean Flow and Turbulence Characteristics in the Annulus-Wall Region of an Axial Flow Compressor Rotor Blade Passage," M. S. Thesis, Dept. of Aerospace Engineering, The Pennsylvania State University, Nov. 1980.